

Evaluating the relationship between the area and latitude of large igneous provinces and Earth's long-term climate state

Yuem Park¹, Nicholas L. Swanson-Hysell¹, Lorraine E. Lisiecki², Francis A. Macdonald²

¹ Department of Earth and Planetary Science, University of California, Berkeley, CA, USA

² Department of Earth Science, University of California, Santa Barbara, CA, USA

This article is in review for the AGU book entitled Environmental Change and Large Igneous Provinces: The Deadly Kiss of LIPs.

¹ ABSTRACT

One of the hypothesized effects of large igneous provinces (LIPs) is planetary cooling on million-year timescales associated with enhanced silicate weathering of the freshly-emplaced basalt. This study combines reconstructions of the original surface extent and emplacement ages of LIPs, a paleogeographic model, and a parameterization of LIP erosion to estimate LIP area in all latitudinal bands through the Phanerozoic. This analysis reveals no significant correlation between total LIP area, nor LIP area in the tropics, and the extent of continental ice sheets. The largest peaks in tropical LIP area are at times of non-glacial climate. These results suggest that changes in planetary weatherability associated with LIPs are not the fundamental control on whether Earth is in a glacial or non-glacial climate, although they could provide a secondary modulating effect in conjunction with other processes.

¹² INTRODUCTION

¹³ Global weatherability is the sum of factors aside from climate itself that contribute to overall
¹⁴ global weathering and associated CO₂ consumption, such as the latitudinal distribution of
¹⁵ continents and mountain belts (Kump and Arthur, 1997). On a planet with high weatherability,
¹⁶ the CO₂ input from volcanism can be removed via silicate weathering at a lower atmospheric CO₂
¹⁷ concentration than on a less weatherable planet. Basaltic regions consume more CO₂ than regions
¹⁸ where the bedrock composition is closer to bulk continental crust because mafic lithologies have
¹⁹ relatively high concentrations of Ca and Mg (that ultimately sequester carbon through
²⁰ precipitation as carbonate), constitute minerals with relatively high reactivity (Gislason and
²¹ Oelkers, 2003), and have relatively high weathering rates (Dessert et al., 2003; Ibarra et al., 2016).
²² Furthermore, data from basaltic watersheds show that chemical weathering rates are highest in
²³ regions with high runoff and temperature. As a result, CO₂ consumption in basaltic regions is
²⁴ most pronounced in the tropical rain belt (Dessert et al., 2003; Hartmann et al., 2009, 2014).

²⁵ One aspect of large igneous province (LIP) emplacement that has been hypothesized to relate
²⁶ to long-term global climate is the effect that associated mafic lithologies could have on increasing
²⁷ global weatherability and driving cooling. In particular, the emplacement of LIPs in the tropics
²⁸ has been hypothesized to be associated with specific episodes of climatic cooling on Earth. In the
²⁹ Neoproterozoic, the emplacement of the ca. 720 Ma Franklin LIP in the tropics, in concert with
³⁰ elevated runoff rates associated with supercontinent break-up, has been implicated as a major
³¹ contributor to the cooling that initiated the Sturtian ‘Snowball Earth’ (Donnadieu et al., 2004a;
³² Macdonald et al., 2010; Cox et al., 2016). In the Cenozoic, the movement of the Deccan LIP into
³³ the tropical rain belt, together with the low-latitude emplacement of the Ethiopian Traps, has
³⁴ been implicated in drawing down CO₂ levels in the lead-up to Oligocene glaciation of Antarctica
³⁵ (Kent and Muttoni, 2008, 2013). More recently, Johansson et al. (2018) used paleogeographic
³⁶ reconstructions to suggest that tropical LIP area correlates with Phanerozoic climate change
³⁷ through comparison with a pCO₂ proxy compilation.

38 This chapter seeks to address two interconnected questions: 1) how unique are the peaks in
39 low-latitude LIP area that have been proposed to be associated with climatic cooling?; and 2)
40 how strong is the overall relationship between tropical LIP area and glaciation?

41 **METHODS**

42 This study combines reconstructions of the original surface extent and emplacement ages of LIPs,
43 a paleogeographic model, and a parameterization of LIP erosion to estimate LIP area in all
44 latitudinal bands through the Phanerozoic. We then compare these time series of zonal LIP area
45 to the latitudinal extent of continental ice sheets - a proxy for Earth's long term climate state.
46 This study builds upon a zonal LIP area analysis presented in the supplementary materials for
47 Macdonald et al. (2019) by more rigorously developing parameterizations of LIP erosion and
48 exploring several geologically reasonable LIP post-emplacement scenarios.

49 Outlines of the original surface extent of continental LIPs through the Phanerozoic (Fig. 1)
50 were slightly modified (to ensure that all currently exposed volcanic lithologies are encapsulated
51 by the initial LIP area polygons) from the compilation of Ernst and Youbi (2017) and Ernst
52 (2019), and emplacement ages were taken from the literature (Table 1). The LIP original surface
53 extent compilation seeks to reconstruct the original surface extent of LIPs with the caveat that
54 there can be significant uncertainty with doing so, particularly for older more deeply eroded LIPs.
55 These polygons encapsulate all of the preserved rocks associated with a given LIP, including
56 dikes, sills, and layered intrusions, in addition to subaerial volcanics (Fig. 1). For some LIPs, this
57 approach may lead to an over-estimate of original surface extent, given that subsurface intrusions
58 could extend over a broader area than the surface volcanics. The polygons also assume complete
59 surface coverage between wide-spread remnants, creating further potential for these original
60 extent outlines to be over-estimates. These original extent outlines could also under-estimate the
61 surface area for some LIPs where flows have been eroded and feeder dikes are not exposed or
62 poorly documented. However, despite these uncertainties, this approach likely provides the best

63 estimates available of original surface extent for ancient LIPs. The extents of presently-exposed
64 volcanics associated with LIPs that were used for present-day area estimates (Fig. 1) and the
65 sources that went into the construction of the original extent polygons by Ernst and Youbi (2017)
66 and Ernst (2019) were taken from a number of resources including the PLATES compilation
67 (Coffin et al., 2006) and more recent compilation efforts associated with the LIPs Reconstruction
68 Project (Ernst et al., 2013; Table 1).

69 After LIPs are emplaced, they progressively erode. In order to account for the associated
70 decrease in area with time, Goddériss et al. (2017b) took the approach of fitting an exponential
71 decay function to estimates of the original surface extent and the current surface extent of 5 LIPs.
72 They used the resulting exponential decay constants to develop a first-order parameterization of
73 changing LIP area through time. We extend this approach to 19 basaltic LIPs for which there are
74 estimates of the original surface extent of the province and the current surface extent of rocks
75 associated with the province (Fig. 2). While there are significant uncertainties associated with
76 the area estimates, this compilation suggests that an exponential decay function is an appropriate
77 first-order representation of the progressive reduction in LIP area (Fig. 2). The best-fit
78 exponential function results in a LIP area half-life of 29 Myr. However, since we explicitly
79 account for LIP burial separately in our area analysis (see below), we exclude from our estimation
80 of a representative LIP area half-life the 6 of 19 LIPs which are inferred to have been partially or
81 completely buried. This latter approach yields a slightly longer best-fit half-life of 36 Myr (Fig.
82 2). Although the exponential fit to the 13 unburied LIPs is good (i.e. it yields a low root mean
83 square error of 0.14), if each LIP is fit individually with an exponential decay function, there is
84 variability in the estimated half-lives from ~20 Myr up to ~120 Myr for the Deccan Traps (Table
85 1). In the analysis of LIP area through time, we implement decay scenarios informed by these
86 results: the ' $t_{1/2} = 36$ Myr' scenario uses the best-fit half-life of 36 Myr, while the ' $t_{1/2} =$
87 120 Myr' scenario uses the slower decay. Given that the post-emplacement weathering and
88 erosional history of each LIP should be dependent on the tectonic and climatic setting that each
89 LIP experiences during and after emplacement, this approach is simplistic, but it provides a

90 framework for analysis. The LIP reconstructions used in this study also include pre-Phanerozoic
91 LIPs. However, given the imposed exponential decay since emplacement, the inclusion of these
92 LIPs does not significantly influence the calculated LIP areas through the Phanerozoic, which is
93 the focus of this analysis.

94 Of the tectonic factors that could alter exposed LIP area, the most consequential is
95 near-immediate burial by sediment of LIP volcanics that are co-located with a rift basin. There
96 are numerous examples in the record where there is partial or complete burial of a LIP associated
97 with rifting and thermal subsidence (Table 1). For example, the Afar LIP is both associated with
98 the Ethiopian Traps which form plateau flood basalts as well as successful rifting in the region of
99 the Red Sea that has resulted in burial (Fig. 1). To account for the rapid decrease in exposed
100 surface area that would result from burial by sediments in a rift basin, we impose two different
101 burial scenarios for LIPs that are co-located with rifting. The ‘50% burial’ scenario imposes
102 instantaneous burial of 50% of the LIP area while the ‘100% burial’ imposes instantaneous burial
103 of the entire LIP as an end-member scenario. A limitation of our treatment of LIPs that are
104 co-located with rifting is that we ‘bury’ all of these LIPs instantly at the time of emplacement
105 and to the same degree when in fact the degree and timing of burial of these LIPs may vary
106 substantially. The LIP area analysis uses all of the available combinations of the distinct decay
107 and burial scenarios described above.

108 Our LIP reconstruction differs from that of Johansson et al. (2018). In contrast to the decay
109 and decay+burial scenarios implemented on estimates of original LIP extent in this study,
110 Johansson et al. (2018) uses a static extent for each LIP throughout the reconstruction. In their
111 analysis, some of the polygons correspond to the present-day surface extent and some represent
112 the original extent that includes currently buried portions of the LIP (e.g. the Keweenawan
113 Midcontinent Rift for which the implemented extent in Johansson et al., 2018 is from geophysical
114 data that largely corresponds to buried subsurface exposures).

115 The original surface extent LIP polygons were assigned a plate ID corresponding to a tectonic

116 unit on Earth using the polygons of Torsvik and Cocks (2016) for the Phanerozoic. The LIP
117 polygons and tectonic units were reconstructed from 520 Ma to the present (e.g. Fig. 5) utilizing
118 the paleogeographic model of Torsvik and Cocks (2016) in the spin axis reference frame (anchor
119 plate ID of 1). This paleogeographic model was updated to include revisions to Ordovician
120 Laurentia (Swanson-Hysell and Macdonald, 2017) and Paleozoic Asia (Domeier, 2018).
121 Reconstructions and area calculations within latitude bands utilized the pyGPlates function
122 library and custom Python scripts. The total LIP area and the LIP area reconstructed within the
123 tropical rain belt were calculated for the various decay and burial scenarios at a resolution of
124 5 Myr (Fig. 4B and C). All the data and code necessary to reproduce the analyses and figures
125 presented in this study can be downloaded from GitHub
126 (https://github.com/Swanson-Hysell-Group/Large_Igneous_Provinces).

127 The ascent of air near the equator associated with Earth's large-scale Hadley circulation
128 promotes precipitation and leads to a low-latitude band of high rainfall known as the tropical rain
129 belt. In contrast, the descending branches of the Hadley circulation in the subtropics are
130 associated with aridity (Manabe, 1969). We use 15° S to 15° N as a working definition of the
131 tropical rain belt, as these latitudes approximately correspond with a sharp increase in zonal
132 mean precipitation when approaching the equator to values greater than 1.0 m/yr in modern
133 climatological data (Kalnay et al., 1996; Fig. 3). Other parameters that could be used to define
134 the tropical rain belt are runoff and precipitation minus evaporation (P-E). When approaching
135 the equator in modern climatological data, zonal mean runoff sharply increases to values above
136 0.25 m/yr between approximately ±10° and ±15° (Fekete et al., 1999; Fig. 3), and zonal mean
137 P-E sharply increases to values above 0.5 m/yr also between approximately ±10° and ±15°
138 (Trenberth et al., 2011; Fig. 3). While seasonally high precipitation within ±15° of the equator
139 associated with migration of the intertropical convergence zone could be a driver of high chemical
140 weathering, annual mean runoff is often the value that is used within parameterizations of
141 chemical weathering (e.g. West, 2012). Using runoff or P-E favors a definition of the tropical rain
142 belt that is closer to ±10° rather than ±15°. Therefore, we tested the sensitivity of our results to

143 the assumed width of the tropical rain belt by performing the tropical LIP area calculations with
144 a tropical rain belt width of $\pm 10^\circ$. We also calculated the area of LIPs within $\pm 20^\circ$ of the equator
145 (a width that includes part of the arid subtropics) in order to account for uncertainties in the
146 paleolatitude of LIPs in the paleogeographic model. We find that both of these additional
147 analyses (LIP area calculated within $\pm 10^\circ$ and $\pm 20^\circ$ of the equator) yield similar results to those
148 obtained when LIP area is calculated within $\pm 15^\circ$ of the equator (Table 2).

149 In Evans (2006), the reconstructed paleolatitudes of basins with thick, basin-wide evaporite
150 deposition are shown to be consistently in the subtropics throughout the Phanerozoic and the
151 Proterozoic, suggesting that the large-scale atmospheric circulation that gives rise to intense
152 precipitation in the tropical rain belt and an arid subtropical climate is stable through time.
153 However, subsequent work by Boucot et al. (2013) and Cao et al. (2018) has interpreted evaporite
154 deposits to have formed at or near the equator at times in the Phanerozoic. While some of this
155 variability could be attributed to waxing/waning of the width of the tropical rain belt as a whole,
156 it is important to note that there can be large deviations in local precipitation from the zonal
157 mean due to factors such as monsoon-related precipitation (Trenberth et al., 2000), or
158 continentality (i.e. how dispersed or amalgamated the continents are) which can lead to aridity in
159 continental interiors. For instance, much of the Early Cretaceous low-latitude evaporite deposits
160 were formed in basins that were located deep within arid continental interiors at the time of
161 deposition (Boucot et al., 2013; Cao et al., 2018). Furthermore, in contrast to Evans (2006), the
162 compilation of evaporite deposits of Boucot et al. (2013) contains sedimentary sequences in which
163 the occurrence of evaporitic minerals is limited (e.g. to disseminated gypsum pseudomorphs).
164 Such limited evaporitic mineral precipitation could be attributed to seasonal evaporation that
165 transiently led to saturation states that otherwise would not be expected for that latitude.
166 Nevertheless, a limitation of the LIP analysis described in this study is that it does not account
167 for deviations in local precipitation from the zonal mean (due to the infeasibility of running a
168 highly-resolved global climate model at each time-step in the analysis). However, evaporite
169 deposits, including those in which the occurrence of evaporitic minerals is limited, are distributed

170 bimodally about the equator in the subtropics for the vast majority of the past \sim 420 Myr (Cao
171 et al., 2018) and overall stability of the large-scale atmospheric circulation is predicted by climate
172 dynamics (Donohoe and Voigt, 2017). Therefore, the assumption of enhanced precipitation and
173 runoff in the tropics throughout the Phanerozoic is warranted.

174 To evaluate the relationship between Earth's climate state and total and tropical LIP area, we
175 compared these areas to a compilation of the latitudinal extent of continental ice sheets over the
176 Phanerozoic (Macdonald et al., 2019; Fig. 4E). The goal in doing so is to evaluate the hypothesis
177 that there is a correlation between LIP area in the tropics and Earth's long-term climate state.
178 The land ice record is an imperfect tracker of climate as it is insensitive to changes in temperature
179 during non-glacial intervals, is influenced by additional factors such as the physical geography of
180 the continents during glacial intervals, and is potentially vulnerable to removal from the
181 observable geologic record via erosion and burial. Furthermore, the threshold $p\text{CO}_2$ for
182 establishing a glacial climate is dependent on ocean circulation and changing solar luminosity (e.g.
183 Shevenell, 2004; DeConto et al., 2008). Nevertheless, it forms a physical record of Earth's climate
184 through time and delineates glacial and non-glacial climate states. We take two approaches for
185 comparison between the LIP area reconstructions and the record of ice extent. The first is to
186 calculate the Pearson correlation coefficient between LIP area and the extent of ice away from the
187 pole. The second is to consider the degree of overlap between intervals of high LIP area (defined
188 as LIP area $>30\%$ of the maximum in a given post-emplacement model) and intervals of glacial
189 climate (defined as ice extent $>10^\circ$ from the poles). This overlap approach places less emphasis on
190 the specific magnitudes of the peaks in the compiled ice extent and LIP area records.

191 Another approach would be to compare the LIP area reconstructions to proxy compilations of
192 $p\text{CO}_2$ (as done by Johansson et al., 2018) instead of the latitudinal extent of continental ice
193 sheets. However, such $p\text{CO}_2$ proxies are potentially problematic as they can be difficult to
194 calibrate in deep time and can be affected by secondary alteration. Even when stringent quality
195 criteria and the latest understanding of each of the $p\text{CO}_2$ proxies have been applied to available

196 $p\text{CO}_2$ records (Foster et al., 2017), both significant uncertainty in the estimated $p\text{CO}_2$ for any
197 given data point as well as disagreement between techniques remain (Fig. 4E). For instance, in
198 the Late Triassic (\sim 240-200 Ma), estimates of $p\text{CO}_2$ span \sim 3000 ppm. Even a probabilistic
199 approach to a large $p\text{CO}_2$ proxy data set can not constrain $p\text{CO}_2$ at the 95% confidence level to
200 within a few hundred ppm for any given time interval, especially when we look deeper in time
201 than the Cenozoic (Foster et al., 2017; Fig. 4E). For the pedogenic carbonate $\delta^{13}\text{C}$ proxy, which
202 forms the majority of the pre-Cenozoic data in the compilation of Foster et al. (2017), such
203 scatter could result from diagenesis (Michel et al., 2016) and the sensitivity of the $p\text{CO}_2$ estimates
204 on assumptions regarding soil-respired CO₂ (Montañez, 2013). Nevertheless, despite these
205 shortcomings, the $p\text{CO}_2$ proxy record is broadly consistent with the ice extent record (Fig. 4E) -
206 $p\text{CO}_2$ proxy data decreases \sim 400-310 Ma as the Late Devonian glacial interval occurs and the
207 Permo-Carboniferous glacial interval begins and waxes, $p\text{CO}_2$ proxy data roughly increases
208 \sim 310-240 Ma as the Permo-Carboniferous glacial interval wanes and ends, $p\text{CO}_2$ proxy data
209 broadly remains relatively high \sim 240-40 Ma when no glacial intervals are robustly documented,
210 and $p\text{CO}_2$ proxy data roughly decreases \sim 40-0 Ma as the Cenozoic glacial interval begins. Given
211 these considerations, we thus prefer to use the latitudinal extent of land ice to reflect Earth's
212 overall climate state throughout the Phanerozoic, despite its own limitations.

213 RESULTS

214 In the ' $t_{1/2} = 36$ Myr' scenario, we observe four main peaks in the calculated LIP area within the
215 tropics (Fig. 4C). The first peak ca. 510 Ma is associated with the emplacement of the
216 Kalkarindji LIP, the second peak ca. 380 Ma is associated with the emplacement of the
217 Kola-Dnieper LIP, the third peak ca. 200 Ma is associated with the emplacement of the Central
218 Atlantic Magmatic Province (CAMP), and the fourth peak is associated with both the ca. 30 Ma
219 emplacement of the Afar LIP as well as the earlier drift of the ca. 66 Ma Deccan LIP into the
220 tropics (Figs. 4A and 5). When we account for burial (' $t_{1/2} = 36$ Myr + 50% burial' and ' $t_{1/2} =$

221 36 Myr + 100% burial' scenarios), only the latter two of these four peaks are affected – the ca.
222 200 Ma peak is attenuated/removed due to the partial/complete burial of the CAMP, and the
223 Cenozoic peak is attenuated due to the partial/complete burial of the Afar LIP. However, after
224 accounting for burial, a minor area of LIPs remain in the tropics from ca. 130 Ma onwards, due
225 to the Equatorial Atlantic Magmatic Province (EQUAMP), Caribbean-Colombian, and Deccan
226 LIPs. Using the longer decay half-life of 120 Myr (the ' $t_{1/2} = 120$ Myr + 100% burial' scenario)
227 increases the area of LIPs in the tropics at any given time step, and has the effect of extending
228 the duration of each peak.

229 The only scenario which results in a non-negative Pearson correlation coefficient (0.10)
230 between LIP area in the tropics ($\pm 15^\circ$; Fig. 4C) and the ice extent record (Fig. 4E) is the
231 scenario with the slow decay rate and complete burial of LIPs associated with rifting (the ' $t_{1/2} =$
232 120 Myr + 100% burial' scenario; Fig. 6). All other scenarios (including both total LIP area and
233 tropical LIP area) yield a near zero or weak negative correlation coefficient (Fig. 6). The weak
234 positive correlation of the ' $t_{1/2} = 120$ Myr + 100% burial' scenario relative to the other scenarios
235 can be primarily attributed to the complete removal of the CAMP, which was emplaced during an
236 extended interval of ice-free conditions, as well as the effect of the longer decay half-life extending
237 the duration of the earlier two peaks, such that they overlap more with the Late Ordovician and
238 Permo-Carboniferous glacial intervals.

239 To assess the statistical significance of the correlation implied by the Pearson correlation
240 coefficients (or lack thereof), we applied the approach of Macdonald et al. (2019) and simulated
241 the four glacial episodes (Fig. 4E) occurring at random times through the past 520 Myr, and
242 recomputed the correlation coefficient and % overlap between the LIP area in the tropics and the
243 randomly timed glacial intervals for each of these 100,000 simulations (Fig. 6). This approach
244 accounts for the fact that spurious correlation can arise between auto-correlated data sets such as
245 these, where each value is not independent, but is instead dependent on the previous state of the
246 system. For the ' $t_{1/2} = 120$ Myr + 100% burial' scenario, 72% of the randomly timed glacial

247 interval simulations correlate better with LIP area in the tropics than the actual ice extent
248 record. With an associated p-value of 0.72, the null hypothesis that glacial intervals do not
249 correlate to LIP area in the tropics cannot be rejected. Taking this approach, none of the positive
250 or negative correlations that emerge between the LIP area scenarios and the ice extent record are
251 statistically significant (Table 2).

252 DISCUSSION

253 In the original models that proposed the ‘Fire and Ice’ hypothesis as an explanation for the onset
254 of the Sturtian ‘Snowball Earth’ glaciation, chemical weathering was modeled as a function of
255 temperature and runoff only (Donnadieu et al., 2004b). However, such an approach neglects the
256 effects of soil shielding and regolith development in low-relief regions. Recent progress on
257 understanding the relationships between landscapes, topography, and chemical weathering reveals
258 that these effects are important (Gabet and Mudd, 2009; Hartmann et al., 2014; Maher and
259 Chamberlain, 2014; Goddériss et al., 2017a). Soil shielding can lead to a transport-limited
260 weathering regime in which the weathering rate of the underlying bedrock becomes insensitive to
261 kinetic and equilibrium factors such as temperature and runoff - factors that would, in the
262 absence of soil shielding, lead to relatively high weathering rates in the tropical rain belt. As a
263 result, more recent modeling of chemical weathering incorporates such processes and highlights
264 the importance of high-relief regions relative to low-relief ones for setting global weatherability
265 (West, 2012; Goddériss et al., 2017a). LIPs are often emplaced in relatively low-relief areas, and as
266 such, without active uplift, soil shielding from regolith development on these low-relief LIPs could
267 significantly decrease the local weatherability of a LIP and mute its impact on global
268 weatherability (as suggested in Kent and Muttoni, 2013). In this way, soil shielding could explain
269 the lack of correlation between tropical LIP area and ice extent (Figs. 4 and 6). In contrast,
270 processes that lead to continued exhumation of mafic lithologies and the creation of steep
271 topography that minimizes soil shielding, particularly in tropical regions, may exert a strong

control on global weatherability and long-term climate. This interpretation underlies the hypothesis that arc-continent collisions in the tropics during the Ordovician (Swanson-Hysell and Macdonald, 2017) and the Cenozoic (Jagoutz et al., 2016) played a significant role in transitions into glacial climate states at those times - a correlation that appears robust throughout the Phanerozoic (Macdonald et al., 2019).

A complication with the interpretation of soil shielding and limited weathering of LIPs is the rapid area decay rate ($t_{1/2} = 36$ Myr) inferred from the comparison of current LIP surface extent to estimated original surface extent (Fig. 2). A couple considerations are relevant with respect to this analysis: 1) the current surface extent of LIP exposure is reduced in part by volcanics being covered by unconsolidated sediments (i.e. regolith development itself) in a number of the provinces; 2) the current surface extent of LIP exposure may be incomplete and an underestimate for some of the provinces; 3) the initial LIP surface extents are typically poorly constrained and are likely over-estimates which could be resulting in inflated interpreted decay rates; and 4) the relationship between LIP area and volume is poorly constrained. Future efforts that improve the LIP database, such as developing better-constrained estimates of original LIP surface extent, constraining burial and uplift histories, and refining the timing of eruptions associated with LIPs, will improve analyses that consider the LIP record in its entirety, such as that in this contribution.

We have focused this analysis on the Phanerozoic record given that well-constrained paleogeographic models are available for the past ~ 520 Myr. The approach of seeking to evaluate correlation between LIP area and glaciation is further complicated for Neoproterozoic Snowball Earth events because ice-albedo runaway leads to persistent global glaciation on timescales of tens of millions of years without continued forcing through normal carbon cycle processes until sufficient CO₂ to drive deglaciation builds up in the absence of silicate weathering (Hoffman et al., 2017). Moreover, cooling past the critical threshold for rapid global glaciation may have occurred on a sub-million year timescale (e.g. Macdonald and Wordsworth, 2017). Nevertheless, evaluating the hypothesis of tropical LIP area associated with the ca. 720 Ma Franklin LIP

298 increasing global weatherability and contributing to the onset of the Sturtian Snowball Earth is a
299 major motivating driver behind conducting this analysis.

300 How does the tropical LIP area associated with the Franklin LIP compare to that observed in
301 the Phanerozoic? Using the paleomagnetic pole of Denyszyn et al. (2009), we reconstruct the
302 paleolatitude of the Franklin LIP at the time of emplacement, and find that ~99.7% (or
303 ~2.6 Mm²) of the LIP erupted within 15° of the equator. This Franklin LIP tropical area at the
304 time of emplacement is approximately equivalent to the Cenozoic peak, and is smaller than the
305 other Phanerozoic peaks (Fig. 4C). The ca. 1109 Ma Umkondo is another Precambrian LIP that
306 is constrained to have erupted in the tropics, although it is not known to be associated with any
307 glaciation (no glacial deposits are found within the contemporaneous Midcontinent Rift basin;
308 Swanson-Hysell et al., 2019). We reconstruct the paleolatitude of the Umkondo LIP at the time of
309 emplacement using the paleomagnetic pole of Swanson-Hysell et al. (2015), and find that
310 effectively all of the LIP (or ~2.0 Mm²) erupted within the tropics, an area that is slightly
311 smaller than that estimated for the Franklin LIP (Fig. 4C).

312 Together, these results indicate that the Franklin LIP, when compared to Phanerozoic as well
313 as other Precambrian LIPs, did not have a uniquely large area in the tropics. Given that similar
314 (and larger) peaks in tropical LIP area are not associated with the onset of glacial periods,
315 additional processes beyond an increase in weatherability due to LIP area in the tropics must
316 have been at play in the initiation of the Sturtian Snowball Earth. One such process could have
317 been unusually high planetary albedo associated with the low-latitude continental configuration of
318 the supercontinent Rodinia (Kirschvink, 1992; Li et al., 2008). However, our analysis of zonal
319 continental area reveals an almost invariant tropical continental area from ~400 Ma to the
320 present (Fig. 7) and consequently no significant correlation between tropical continental area and
321 the ice extent record in the Phanerozoic, although it is intriguing that there is a high and rising
322 low-latitude continental area in the Ordovician. Similar to the LIP area analysis, this continental
323 area analysis suggests that a low-latitude continental configuration can not be invoked as the sole

324 driver of planetary cooling, although it could be a contributing factor. Another potential
325 contributing process for Neoproterozoic cooling leading up to the Sturtian glaciation is an
326 increase in global weatherability associated with the collision and accretion of arc terranes within
327 the present-day Arabian-Nubian Shield (Park et al., in review). Together, a low-latitude
328 continental configuration and abundant arc-continent collisions in the tropics may have led to a
329 cool background climate, and the emplacement of the Franklin LIP may have further increased
330 global weatherability to the point where the ice-albedo runaway could take effect. However,
331 tropical LIP area associated with the Franklin was not uniquely high, and therefore an associated
332 increase in global weatherability was likely not the sole driver of Snowball Earth onset, consistent
333 with the results of the Phanerozoic analysis.

334 The temporal overlap between Franklin LIP eruptions and the initiation of Sturtian glaciation
335 remains compelling (Macdonald et al., 2010; MacLennan et al., 2018). This overlap could support
336 arguments that other aspects of LIP emplacement, such as the injection of sulfur aerosols in the
337 stratosphere (Macdonald and Wordsworth, 2017), played a role in the initiation of low-latitude
338 glaciation. The temporary effect on albedo of such aerosols is maximized when they are injected
339 into the atmosphere at low-latitudes into a cool background climate and their presence at high
340 concentrations is pre-conditioned on eruption through sedimentary basins hosting evaporite
341 deposits, as could have been the case for the Franklin LIP (Macdonald and Wordsworth, 2017).
342 However, in the cases in which such aerosol-driven cooling does not result in ice-albedo runaway
343 and a Snowball Earth, the climate would return to its background climate state within years
344 (Macdonald and Wordsworth, 2017). A contrasting effect is that, on 1 kyr to 1 Myr timescales,
345 LIP emplacement could instead cause transient warming associated with elevated CO₂ outgassing
346 leading to transiently high pCO₂, as has been argued for the CAMP (Schaller et al., 2011, 2012).

347 The results from this analysis indicate that when the entire LIP database is considered in
348 conjunction with a paleogeographic reconstruction and this parameterization of erosion, there is
349 no significant relationship between total LIP area nor LIP area in the tropics and the extent of

350 continental ice sheets. While this result need not imply that there is no increase in global
351 weatherability from the emplacement of LIPs, it does suggest that changes in planetary
352 weatherability associated with LIPs are not the fundamental control on whether Earth is in a
353 glacial or non-glacial climate state.

354 **ACKNOWLEDGEMENTS**

355 Richard Ernst provided GIS compilations of LIP extent and present-day exposure that were
356 essential to the analysis. Discussions with Yves Goddériss made possible through the
357 France-Berkeley Fund contributed valuably to aspects of the interpretation. Park was supported
358 by NSF Grant 1547434 awarded to Swanson-Hysell.

359 **TABLES**

Table 1. Phanerozoic large igneous provinces (and the Franklin).

name	age (Ma)	age ref.	original ¹ area (Mm ²)	present ² area (Mm ²)	present area ref.	present ³ / original	half-life ⁴ (Myr)	buried?
Columbia River	16	Kasbohm and Schoene (2018)	0.68	0.38	Buchan and Ernst (2004)	0.56	19.2	no
Afar	30	Courtillot and Renne (2003)	2.05	0.63	Coffin et al. (2006)	0.31	17.7	partial
NAIP	62	Larsen et al. (2015)	1.07	0.29	Buchan and Ernst (2004); Coffin et al. (2006)	0.27	33.0	partial
Deccan	66	Schoene et al. (2014)	0.83	0.56	Coffin et al. (2006)	0.68	116.6	no
Seychelles	66	Schoene et al. (2014)	0.46	0.00	Coffin et al. (2006)	0.00	0.0	yes
Madagascar	90	Cucciniello (2010)	0.63	0.03	Coffin et al. (2006)	0.05	20.8	no
Caribbean-Colombian	94	Loewen et al. (2013)	0.71	0.13	Coffin et al. (2006)	0.18	37.6	no
HALIP	95	Kingsbury et al. (2018)	3.60	0.15	Hartmann and Moosdorf (2012)	0.04	20.7	no
EQUAMP	131	Hollanda et al. (2016)	0.66	0.01	Hollanda et al. (2016)	0.01	20.5	no
Comei	132	Zhu et al. (2009)	0.11	-	-	-	-	no
Bunbury	132	Zhu et al. (2009)	0.03	0.00	Thorne et al. (2014)	0.05	30.9	no
Parana-Etendeka	135	Florisbal et al. (2014); Almeida et al. (2018)	3.12	0.40	Coffin et al. (2006)	0.13	45.7	partial
Trap	140	Ernst and Buchan (2001)	0.03	0.00	Ernst and Buchan (2001)	0.00	0.0	no
NW Australia Margin	160	Pirajno and Hoatson (2012)	0.62	0.00	Coffin et al. (2006)	0.00	0.0	yes
Karoo	183	Burgess et al. (2015)	3.21	0.15	de Kock compilation ⁵	0.05	41.3	no
Ferrar	183	Burgess et al. (2015)	0.18	-	-	-	-	no
CAMP	201	Blackburn et al. (2013)	11.46	0.23	Marzoli and Parisio compilation ⁶	0.02	35.7	partial
Siberia	252	Burgess and Bowring (2015)	3.46	0.47	Coffin et al. (2006)	0.14	87.5	no
Emeishan	259	Zhou et al. (2002)	0.71	0.06	Coffin et al. (2006)	0.09	72.9	no
Panjal-Qiangtang	283	Zhai et al. (2013)	0.11	-	-	-	-	no
Tarim	290	Xu et al. (2014)	0.35	-	-	-	-	no
Magdalen	360	Murphy et al. (1999)	0.42	-	-	-	-	no
Vilyui	374	Ricci et al. (2013)	1.14	-	-	-	-	no
Kola-Dnieper	380	Arzamastsev and Wu (2014)	5.90	-	-	-	-	no
Suordakh	450	Khudoley et al. (2013)	0.02	-	-	-	-	no
Kalkarindji	511	Jourdan et al. (2014)	3.54	0.17	Thorne et al. (2014)	0.05	116.3	no
Franklin	720	Denyszyn et al. (2009)	2.62	0.04	Buchan and Ernst (2004)	0.02	121.8	no

¹obtained via calculating the area of the continental portions of polygons within the LIP original surface extent compilation of Ernst and Youbi (2017) and Ernst (2019), shown as blue polygons in Fig. 1.

²obtained via calculating the area of polygons from the noted reference of presently-exposed volcanics associated with LIPs, shown as orange polygons in Fig. 1.

³present area / original area

⁴assuming exponential decay with form $N(t) = 2^{t/t_{1/2}}$.

⁵from ArcGIS compilation produced by M. de Kock for the LIPs Reconstruction Project (Ernst et al., 2013).

⁶from ArcGIS compilation produced by A. Marzoli and L. Parisio for the LIPs Reconstruction Project (Ernst et al., 2013).

Table 2. Statistics of correlation between large igneous province area and ice extent.

scenario	within tropics $\pm 15^\circ$				total ⁵				within tropics $\pm 10^\circ$				within tropics $\pm 20^\circ$			
	correlation ¹ val. ³	p-val. ⁴	% overlap ² val.	p-val.	correlation val.	p-val.	% overlap val.	p-val.	correlation val.	p-val.	% overlap val.	p-val.	correlation val.	p-val.	% overlap val.	p-val.
$t_{1/2} = 36$ Myr	-0.19	0.81	13	0.94	-0.26	0.85	30	0.95	-0.22	0.86	13	0.95	-0.17	0.77	9	0.96
$t_{1/2} = 36$ Myr + 50% burial	-0.14	0.73	22	0.85	-0.25	0.84	52	0.97	-0.17	0.79	9	0.90	-0.10	0.67	26	0.86
$t_{1/2} = 36$ Myr + 100% burial	-0.02	0.45	22	0.65	-0.14	0.74	65	0.94	-0.08	0.54	9	0.76	0.04	0.37	22	0.65
$t_{1/2} = 120$ Myr + 100% burial	0.10	0.32	35	0.72	0.00	0.51	100	1.00	0.02	0.40	26	0.77	0.19	0.24	48	0.66

¹Pearson correlation coefficient between LIP area and the actual ice extent record.

²% of time when both LIP area is >30% of the maximum and ice extent is > 10° from the poles.

³'val.' refers to the computed correlation coefficient/% overlap between LIP area and the actual ice extent record.

⁴'p-val.' refers to the fraction of randomly timed glacial interval simulations that correlate/overlap better with LIP area than the actual ice extent record (i.e. the p-value with respect to the null hypothesis of no correlation/overlap). P-values <0.05 indicate that we can reject the null hypothesis at the 95% confidence level.

⁵all latitudes.

360 **FIGURES**

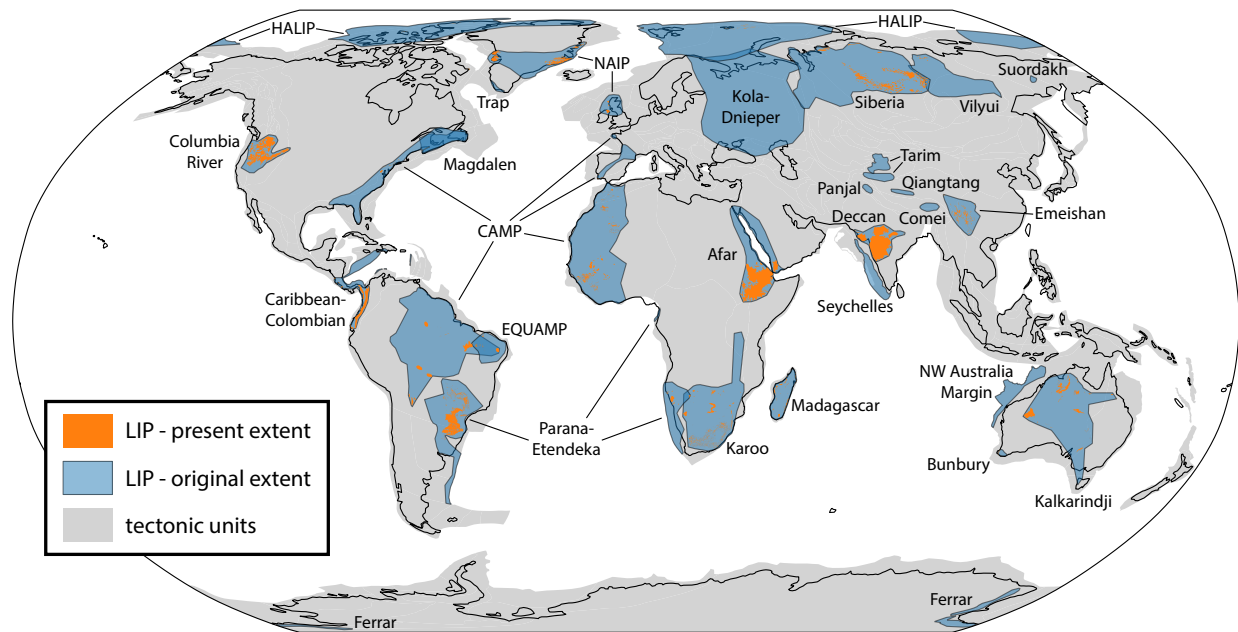


Figure 1. Map of current surface extent of volcanic lithologies associated with LIPs that erupted between 520 Ma and the present, as well as the estimates of the initial LIP surface extent used in the area analysis (modified slightly from Ernst and Youbi, 2017 and Ernst, 2019 to ensure that all currently exposed volcanic lithologies are encapsulated by the initial LIP surface area polygons).

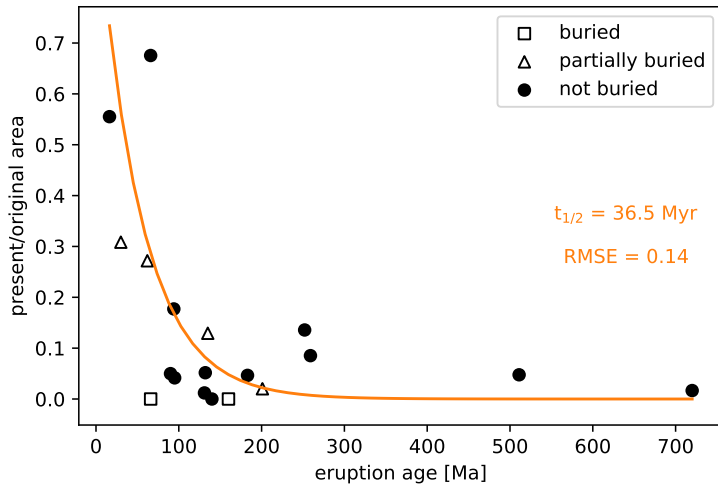


Figure 2. LIP erosion through time. The ratio of estimates of the present-day surface area to that of the original surface area are shown for 19 basaltic LIPs. An exponential fit is made to the 13 basaltic LIPs that are interpreted to not have been buried after emplacement (Table 1), which yields a half-life of ~ 36 Myr. RMSE = root mean square error.

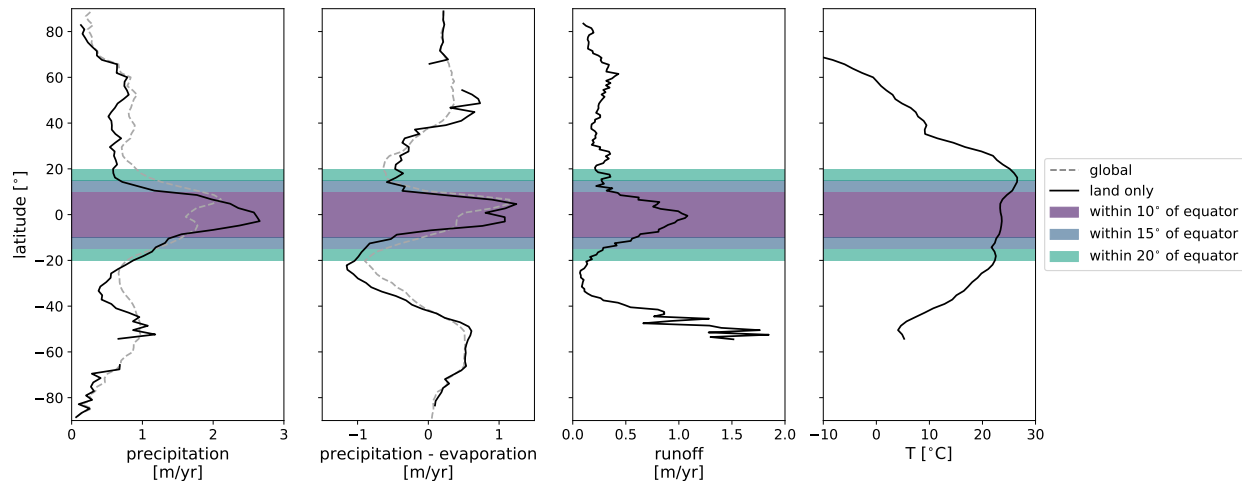


Figure 3. Zonally averaged modern climatological data used to define the tropical rain belt. The global precipitation (Kalnay et al., 1996) and precipitation minus evaporation (Trenberth et al., 2011) data include land and ocean pixels, global temperature data (Kalnay et al., 1996) are from land only, and runoff data (Fekete et al., 1999) are from land only excluding Antarctica. The peak in runoff $\sim 50^\circ$ is due to anomalously high orographically-induced runoff in the southern Andes, which represents almost all of the land in that latitude belt. Temperature data for Antarctica are off scale. Precipitation, precipitation minus evaporation, and runoff all increase sharply between $\pm 10^\circ$ and $\pm 15^\circ$.

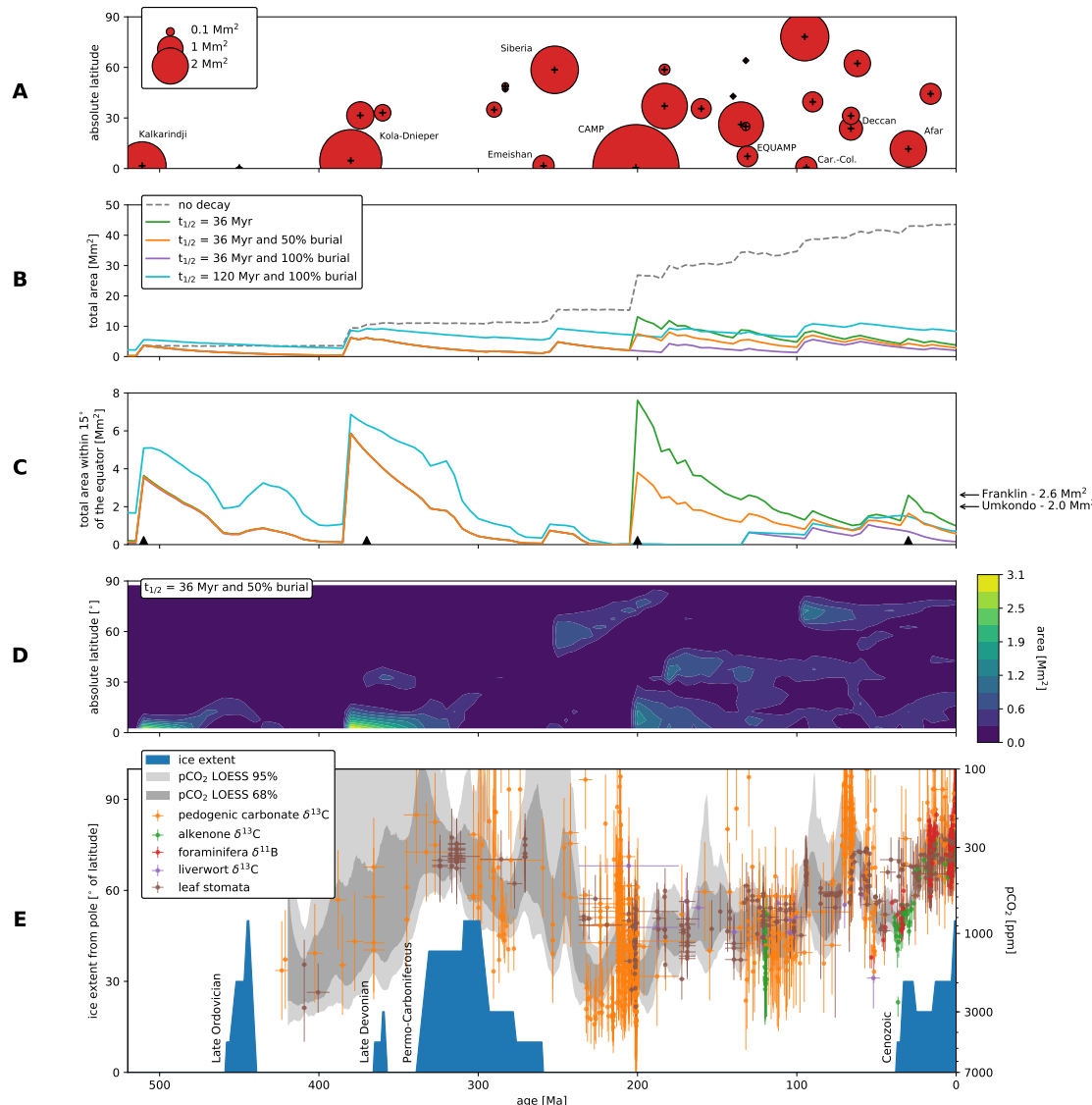


Figure 4. **A)** LIPs included in this analysis. The size of each circle reflects the initial surface area estimate of each LIP. The + indicates the timing and absolute paleolatitude of the centroid of each LIP at the time of emplacement. Car.-Col. = Caribbean-Colombian. **B)** Total LIP area through time for the different post-emplacement scenarios. Only the ‘no decay’ scenario excludes pre-Phanerozoic LIPs. **C)** Tropical LIP area through time for the different post-emplacement scenarios. The arrows to the right indicate reconstructed tropical LIP area at the time of emplacement for the ca. 720 and 1109 Ma Franklin and Umkondo LIPs. The triangles show the paleogeographic reconstruction times in Fig. 5. **D)** Contour plot showing the latitudinal distribution of LIP area for one of the post-emplacement models. **E)** Latitudinal extent of land ice away from the poles (Macdonald et al., 2019) and compilation of $p\text{CO}_2$ proxies (Foster et al., 2017) ($p\text{CO}_2$ y-axis reversed, and in log-scale). Error bars indicate standardized uncertainties, and grey bands indicate 68 and 95% confidence intervals for Monte Carlo resampled LOESS fits to the $p\text{CO}_2$ proxy data (Foster et al., 2017). Note that there are $p\text{CO}_2$ proxy estimates <100 ppm that are cut off in this plot.

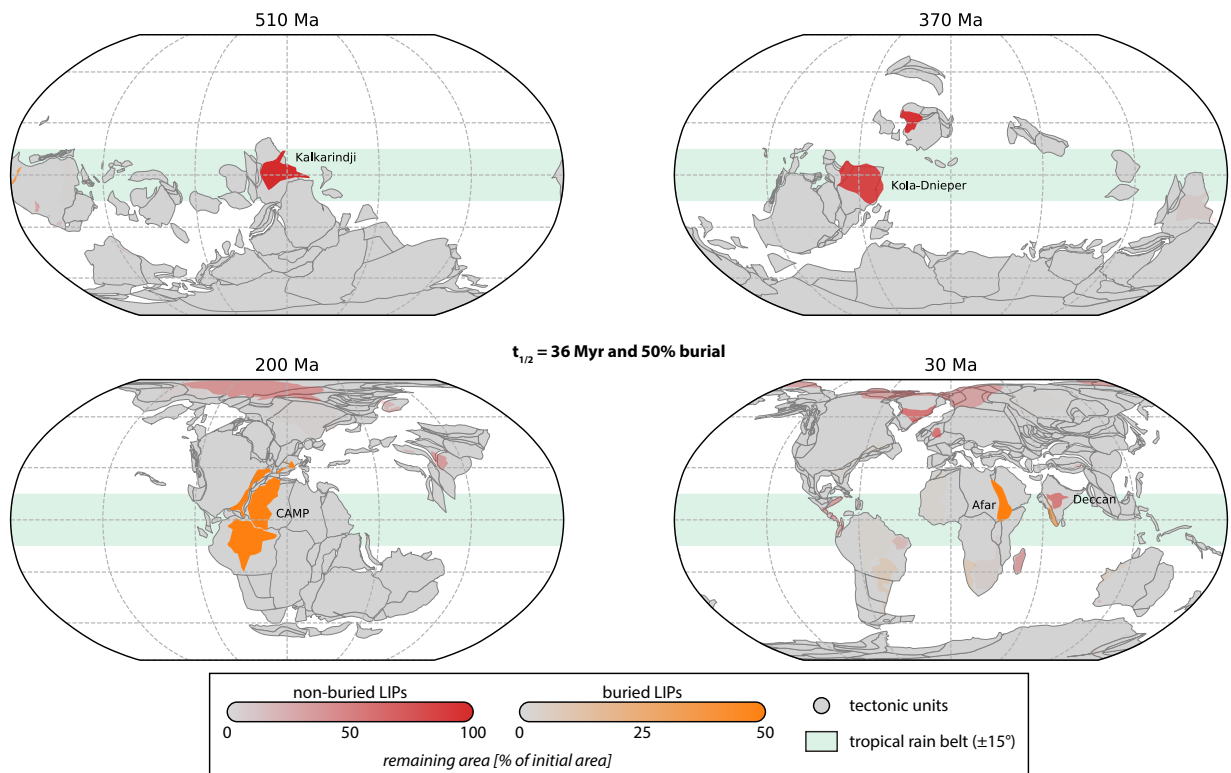


Figure 5. Paleogeographic reconstructions for times that correspond to peaks of LIP area in the tropics (Fig. 4C). The opacity of LIP polygons indicates their parameterized remaining area at the time of the reconstruction as a percentage of initial LIP area, under the preferred post-emplacement scenario of ' $t_{1/2} = 36 \text{ Myr} + 50\% \text{ burial}$ '.

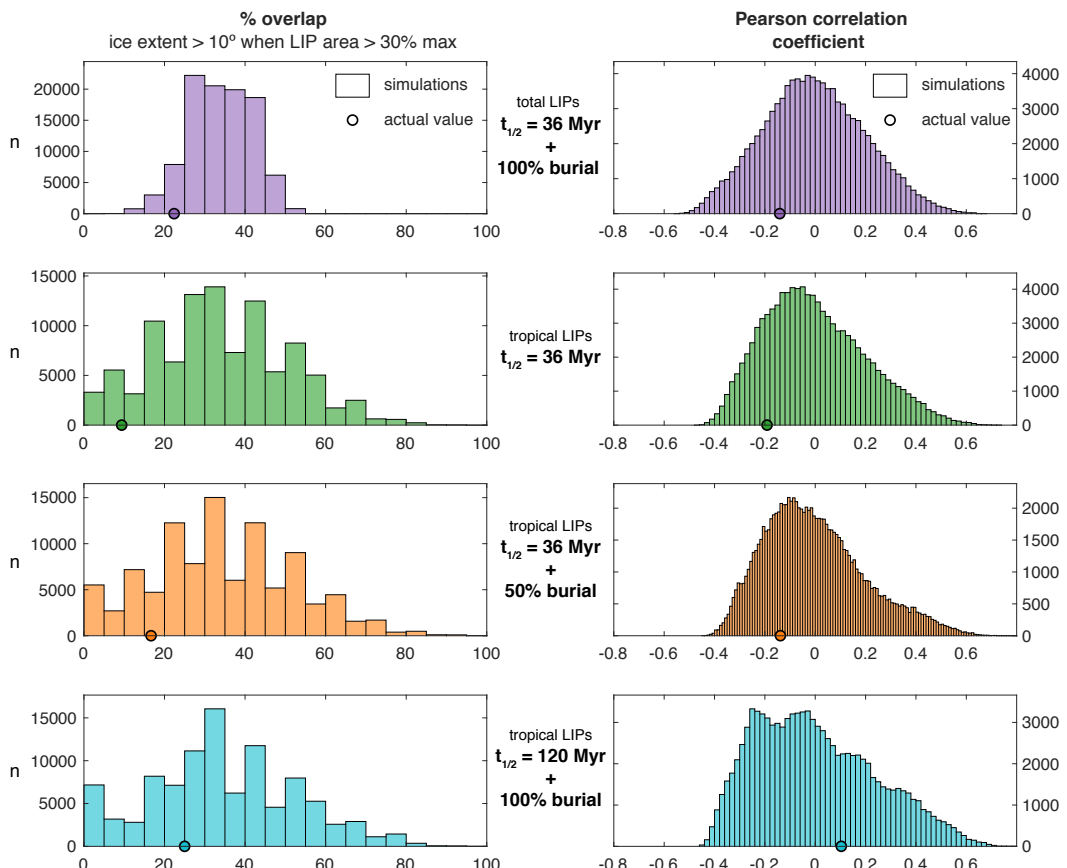


Figure 6. The % overlap and Pearson correlation coefficients between LIP area and the actual ice-extent record are shown with circles. These values are compared to histograms that show the range of values that arise when comparing the LIP area record to glacial intervals that have been shifted randomly in time 100,000 times. The fraction of randomly timed glacial interval simulations that correlate/overlap better with LIP area than the actual ice-extent record is the p-value shown in Table 2.

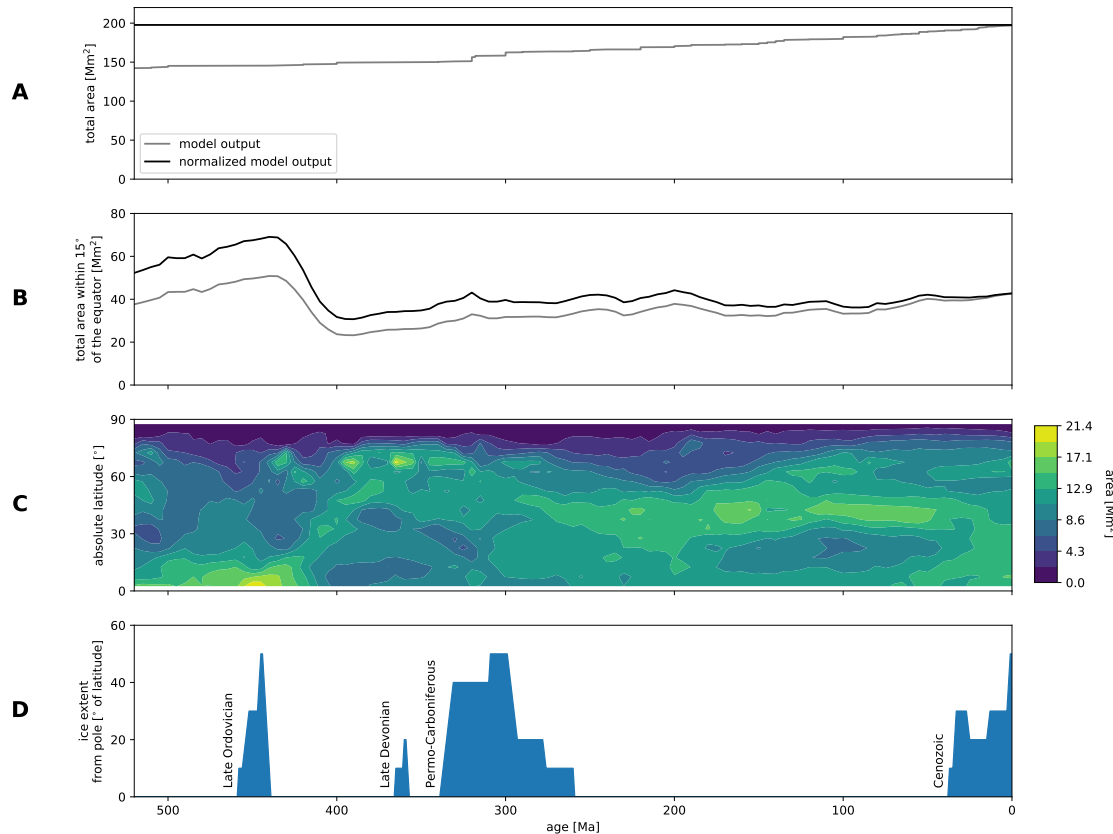


Figure 7. **A)** Total continental area through time. In the paleogeographic model used in this study, tectonic units (Torsvik and Cocks, 2016) are progressively added to the model, leading to a net increase in total continental area in the model of $\sim 33\%$ over the Phanerozoic. However, estimates of continental crust growth (e.g. Pujol et al., 2013) suggest that continental area was roughly constant through the Phanerozoic. We therefore normalize the total continental area curve in our model by assuming a fixed continental area through the Phanerozoic. **B)** Tropical continental area through time. We normalize the tropical continental area curve using the normalization ratio implied in (A). **C)** Contour plot showing the latitudinal distribution of continental area. **D)** Latitudinal extent of land ice away from the poles (Macdonald et al., 2019).

361 References

- 362 Almeida, V. V., Janasi, V. A., Heaman, L. M., Shaulis, B. J., Hollanda, M. H. B., and Renne, P. R., 2018,
363 Contemporaneous alkaline and tholeiitic magmatism in the Ponta Grossa Arch, Paraná-Etendeka Magmatic
364 Province: Constraints from U-Pb zircon/baddeleyite and $^{40}\text{Ar}/^{39}\text{Ar}$ phlogopite dating of the José Fernandes
365 Gabbro and mafic dykes: Journal of Volcanology and Geothermal Research, vol. 355, pp. 55–65,
366 doi:10.1016/j.jvolgeores.2017.01.018.
- 367 Arzamastsev, A. A. and Wu, F.-Y., 2014, U-Pb geochronology and Sr-Nd isotopic systematics of minerals from the
368 ultrabasic-alkaline massifs of the Kola province: Petrology, vol. 22, pp. 462–479, doi:10.1134/s0869591114050026.
- 369 Blackburn, T. J., Olsen, P. E., Bowring, S. A., McLean, N. M., Kent, D. V., Puffer, J., McHone, G., Rasbury, E. T.,
370 and Et-Touhami, M., 2013, Zircon U-Pb geochronology links the End-Triassic extinction with the Central
371 Atlantic Magmatic Province: Science, vol. 340, pp. 941–945, doi:10.1126/science.1234204.
- 372 Boucot, A. J., Xu, C., Scotese, C. R., and Morley, R. J., 2013, Phanerozoic Paleoclimate: An Atlas of Lithologic
373 Indicators of Climate: SEPM (Society for Sedimentary Geology), doi:10.2110/sepmcsp.11.
- 374 Buchan, K. L. and Ernst, R. E., 2004, Diabase dyke swarms and related units in Canada and adjacent regions:
375 Geological Survey of Canada Map 2022A, doi:10.4095/214883.
- 376 Burgess, S. D. and Bowring, S. A., 2015, High-precision geochronology confirms voluminous magmatism before,
377 during, and after Earth's most severe extinction: Science Advances, vol. 1, pp. 1–14, doi:10.1126/sciadv.1500470.
- 378 Burgess, S. D., Bowring, S. A., Fleming, T. H., and Elliot, D. H., 2015, High-precision geochronology links the
379 Ferrar large igneous province with early-Jurassic ocean anoxia and biotic crisis: Earth and Planetary Science
380 Letters, vol. 415, pp. 90–99, doi:10.1016/j.epsl.2015.01.037.
- 381 Cao, W., Williams, S., Flament, N., Zahirovic, S., Scotese, C., and Müller, R. D., 2018, Palaeolatitudinal
382 distribution of lithologic indicators of climate in a palaeogeographic framework: Geological Magazine, vol. 156,
383 pp. 331–354, doi:10.1017/s0016756818000110.
- 384 Coffin, M., Duncan, R., Eldholm, O., Fitton, J. G., Frey, F., Larsen, H. C., Mahoney, J., Saunders, A., Schlich, R.,
385 and Wallace, P., 2006, Large igneous provinces and scientific ocean drilling: Status quo and a look ahead:
386 Oceanography, vol. 19, pp. 150–160, doi:10.5670/oceanog.2006.13.
- 387 Courtillot, V. E. and Renne, P. R., 2003, On the ages of flood basalt events: Comptes Rendus Geoscience, vol. 335,
388 pp. 113–140, doi:10.1016/s1631-0713(03)00006-3.
- 389 Cox, G. M., Halverson, G. P., Stevenson, R. K., Vokaty, M., Poirier, A., Kunzmann, M., Li, Z.-X., Denyszyn, S. W.,
390 Strauss, J. V., and Macdonald, F. A., 2016, Continental flood basalt weathering as a trigger for Neoproterozoic
391 Snowball Earth: Earth and Planetary Science Letters, vol. 446, pp. 89–99, doi:10.1016/j.epsl.2016.04.016.
- 392 Cucciniello, C., 2010, U-Pb ages, Pb-Os isotope ratios, and platinum-group element (PGE) composition of the
393 West-Central Madagascar flood basalt province: The Journal of Geology, vol. 118, pp. 523–541,
394 doi:10.1086/655012.
- 395 DeConto, R. M., Pollard, D., Wilson, P. A., Pälike, H., Lear, C. H., and Pagani, M., 2008, Thresholds for Cenozoic
396 bipolar glaciation: Nature, vol. 455, pp. 652–656, doi:10.1038/nature07337.
- 397 Denyszyn, S. W., Halls, H. C., Davis, D. W., and Evans, D. A., 2009, Paleomagnetism and U-Pb geochronology of
398 Franklin dykes in High Arctic Canada and Greenland: a revised age and paleomagnetic pole constraining block
399 rotations in the Nares Strait region: Canadian Journal of Earth Sciences, vol. 46, pp. 689–705,
400 doi:10.1139/E09-042.
- 401 Dessert, C., Dupré, B., Gaillardet, J., François, L. M., and Allègre, C. J., 2003, Basalt weathering laws and the
402 impact of basalt weathering on the global carbon cycle: Chemical Geology, vol. 202, pp. 257–273,
403 doi:10.1016/j.chemgeo.2002.10.001.

- 404 Domeier, M., 2018, Early Paleozoic tectonics of Asia: Towards a full-plate model: Geoscience Frontiers, vol. 9, pp.
405 789–862, doi:10.1016/j.gsf.2017.11.012.
- 406 Donnadieu, Y., Godderis, Y., Ramstein, G., Nedelev, A., and Meert, J., 2004a, A ‘snowball Earth’ climate triggered
407 by continental break-up through changes in runoff: Nature, vol. 428, pp. 303–306.
- 408 Donnadieu, Y., Ramstein, G., Fluteau, F., Roche, D., and Ganopolski, A., 2004b, The impact of atmospheric and
409 oceanic heat transports on the sea-ice-albedo instability during the Neoproterozoic: Climate Dynamics, vol. 22,
410 pp. 293–306, doi:10.1007/s00382-003-0378-5.
- 411 Donohoe, A. and Voigt, A., 2017, Why future shifts in tropical precipitation will likely be small: Geophysical
412 Monograph Series, pp. 115–137, doi:10.1002/9781119068020.ch8.
- 413 Ernst, R. E., 2019, Introduction to environmental change and large igneous provinces: The deadly kiss of LIPs: In
414 Environmental Change and Large Igneous Provinces: The Deadly Kiss of LIPs, American Geophysical Union.
- 415 Ernst, R. E., Bleeker, W., Söderlund, U., and Kerr, A. C., 2013, Large igneous provinces and supercontinents:
416 Toward completing the plate tectonic revolution: Lithos, vol. 174, pp. 1–14, doi:10.1016/j.lithos.2013.02.017.
- 417 Ernst, R. E. and Buchan, K. L., 2001, Large mafic magmatic events through time and links to mantle-plume heads:
418 In Special Paper 352: Mantle plumes: their identification through time, Geological Society of America, pp.
419 483–575, doi:10.1130/0-8137-2352-3.483.
- 420 Ernst, R. E. and Youbi, N., 2017, How large igneous provinces affect global climate, sometimes cause mass
421 extinctions, and represent natural markers in the geological record: Palaeogeography, Palaeoclimatology,
422 Palaeoecology, vol. 478, pp. 30–52, doi:10.1016/j.palaeo.2017.03.014.
- 423 Evans, D. A. D., 2006, Proterozoic low orbital obliquity and axial-dipolar geomagnetic field from evaporite
424 palaeolatitudes: Nature, vol. 444, pp. 51–55, doi:10.1038/nature05203.
- 425 Fekete, B. M., Vörösmarty, C. J., and Grabs, W., 1999, Global, composite runoff fields based on observed river
426 discharge and simulated water balances: Global Runoff Data Centre Koblenz, Germany.
- 427 Florisbal, L. M., Heaman, L. M., de Assis Janasi, V., and de Fatima Bitencourt, M., 2014, Tectonic significance of
428 the Florianópolis Dyke Swarm, Paraná-Etendeka Magmatic Province: A reappraisal based on precise U-Pb
429 dating: Journal of Volcanology and Geothermal Research, vol. 289, pp. 140–150,
430 doi:10.1016/j.jvolgeores.2014.11.007.
- 431 Foster, G. L., Royer, D. L., and Lunt, D. J., 2017, Future climate forcing potentially without precedent in the last
432 420 million years: Nature Communications, vol. 8, p. 14,845, doi:10.1038/ncomms14845.
- 433 Gabet, E. J. and Mudd, S. M., 2009, A theoretical model coupling chemical weathering rates with denudation rates:
434 Geology, vol. 37, pp. 151–154, doi:10.1130/G25270A.1.
- 435 Gislason, S. R. and Oelkers, E. H., 2003, Mechanism, rates, and consequences of basaltic glass dissolution: II. an
436 experimental study of the dissolution rates of basaltic glass as a function of pH and temperature: Geochimica et
437 Cosmochimica Acta, vol. 67, pp. 3817–3832, doi:10.1016/s0016-7037(03)00176-5.
- 438 Goddérés, Y., Donnadieu, Y., Carretier, S., Aretz, M., Dera, G., Macouin, M., and Regard, V., 2017a, Onset and
439 ending of the late Palaeozoic ice age triggered by tectonically paced rock weathering: Nature Geoscience, vol. 10,
440 pp. 382–386, doi:10.1038/ngeo2931.
- 441 Goddérés, Y., Hir, G. L., Macouin, M., Donnadieu, Y., Hubert-Théou, L., Dera, G., Aretz, M., Fluteau, F., Li,
442 Z. X., and Halverson, G. P., 2017b, Paleogeographic forcing of the strontium isotopic cycle in the Neoproterozoic:
443 Gondwana Research, vol. 42, pp. 151–162, doi:10.1016/j.gr.2016.09.013.

- 444 Hartmann, J., Jansen, N., Dürr, H. H., Kempe, S., and Köhler, P., 2009, Global CO₂-consumption by chemical
445 weathering: What is the contribution of highly active weathering regions?: *Global and Planetary Change*,
446 vol. 69, pp. 185–194, doi:10.1016/j.gloplacha.2009.07.007.
- 447 Hartmann, J. and Moosdorf, N., 2012, The new global lithological map database GLiM: A representation of rock
448 properties at the Earth surface: *Geochemistry, Geophysics, Geosystems*, vol. 13, doi:10.1029/2012GC004370.
- 449 Hartmann, J., Moosdorf, N., Lauerwald, R., Hinderer, M., and West, A. J., 2014, Global chemical weathering and
450 associated P-release - the role of lithology, temperature and soil properties: *Chemical Geology*, vol. 363, pp.
451 145–163, doi:10.1016/j.chemgeo.2013.10.025.
- 452 Hoffman, P. F., Abbot, D. S., Ashkenazy, Y., Benn, D. I., Brocks, J. J., Cohen, P. A., Cox, G. M., Creveling, J. R.,
453 Donnadieu, Y., Erwin, D. H., Fairchild, I. J., Ferreira, D., Goodman, J. C., Halverson, G. P., Jansen, M. F.,
454 Le Hir, G., Love, G. D., Macdonald, F. A., Maloof, A. C., Partin, C. A., Ramstein, G., Rose, B. E. J., Rose,
455 C. V., Sadler, P. M., Tziperman, E., Voigt, A., and Warren, S. G., 2017, Snowball Earth climate dynamics and
456 Cryogenian geology-geobiology: *Science Advances*, vol. 3, doi:10.1126/sciadv.1600983.
- 457 Hollanda, M. H. B. M., Archanjo, C. J., Renne, P. R., Ngonge, D. E., Castro, D. L., Oliveira, D. C., and
458 Macêdo Filho, A. A., 2016, Evidence of an Early Cretaceous giant dyke swarm in northeast Brazil (South
459 America): A geodynamic overview: *Acta Geologica Sinica - English Edition*, vol. 90, pp. 109–110,
460 doi:10.1111/1755-6724.12915.
- 461 Ibarra, D. E., Caves, J. K., Moon, S., Thomas, D. L., Hartmann, J., Chamberlain, C. P., and Maher, K., 2016,
462 Differential weathering of basaltic and granitic catchments from concentration-discharge relationships:
463 *Geochimica et Cosmochimica Acta*, vol. 190, pp. 265 – 293, doi:10.1016/j.gca.2016.07.006.
- 464 Jagoutz, O., Macdonald, F. A., and Royden, L., 2016, Low-latitude arc-continent collision as a driver for global
465 cooling: *Proceedings of the National Academy of Sciences*, vol. 113, pp. 4935–4940, doi:10.1073/pnas.1523667113.
- 466 Johansson, L., Zahirovic, S., and Müller, R. D., 2018, The interplay between the eruption and weathering of large
467 igneous provinces and the deeptime carbon cycle: *Geophysical Research Letters*, vol. 45,
468 doi:10.1029/2017GL076691.
- 469 Jourdan, F., Hodges, K., Sell, B., Schaltegger, U., Wingate, M., Evins, L., Söderlund, U., Haines, P., Phillips, D.,
470 and Blenkinsop, T., 2014, High-precision dating of the Kalkarindji large igneous province, Australia, and
471 synchrony with the Early-Middle Cambrian (Stage 4-5) extinction: *Geology*, vol. 42, pp. 543–546,
472 doi:10.1130/g35434.1.
- 473 Kalnay, E., Kanamitsu, M., Kistler, R., Collins, W., Deaven, D., Gandin, L., Iredell, M., Saha, S., White, G.,
474 Woollen, J., and et al., 1996, The NCEP/NCAR 40-year reanalysis project: *Bulletin of the American
475 Meteorological Society*, vol. 77, pp. 437–471, doi:10.1175/1520-0477(1996)077<437:tnyrp>2.0.co;2.
- 476 Kasbohm, J. and Schoene, B., 2018, Rapid eruption of the Columbia River flood basalt and correlation with the
477 mid-Miocene climate optimum: *Science Advances*, vol. 4, pp. 1–8, doi:10.1126/sciadv.aat8223.
- 478 Kent, D. V. and Muttoni, G., 2008, Equatorial convergence of india and early Cenozoic climate trends: *Proceedings
479 of the National Academy of Sciences*, vol. 105, pp. 16,065–16,070, doi:10.1073/pnas.0805382105.
- 480 Kent, D. V. and Muttoni, G., 2013, Modulation of Late Cretaceous and Cenozoic climate by variable drawdown of
481 atmospheric pCO₂ from weathering of basaltic provinces on continents drifting through the equatorial humid
482 belt: *Climate of the Past*, vol. 9, pp. 525–546, doi:10.5194/cp-9-525-2013.
- 483 Khudoley, A. K., Prokopiev, A. V., Chamberlain, K. R., Ernst, R. E., Jowitt, S. M., Malyshev, S. V., Zaitsev, A. I.,
484 Kropachev, A. P., and Koroleva, O. V., 2013, Early Paleozoic mafic magmatic events on the eastern margin of
485 the Siberian craton: *Lithos*, vol. 174, pp. 44–56, doi:10.1016/j.lithos.2012.08.008.

- 486 Kingsbury, C. G., Kamo, S. L., Ernst, R. E., Söderlund, U., and Cousens, B. L., 2018, U-Pb geochronology of the
487 plumbing system associated with the Late Cretaceous Strand Fiord Formation, Axel Heiberg Island, Canada:
488 part of the 130–90 Ma High Arctic large igneous province: *Journal of Geodynamics*, vol. 118, pp. 106–117,
489 doi:10.1016/j.jog.2017.11.001.
- 490 Kirschvink, J. L., 1992, Late Proterozoic low-latitude global glaciation: The Snowball Earth: *In* Schopf, J., Klein,
491 C., and Des Maris, D., eds., *The Proterozoic Biosphere: A Multidisciplinary Study*, Cambridge University Press,
492 pp. 51–52.
- 493 Kump, L. R. and Arthur, M. A., 1997, Global Chemical Erosion during the Cenozoic: Weatherability Balances the
494 Budgets, Springer US, Boston, MA, pp. 399–426: doi:10.1007/978-1-4615-5935-1_18.
- 495 Larsen, L. M., Pedersen, A. K., Tegner, C., Duncan, R. A., Hald, N., and Larsen, J. G., 2015, Age of Tertiary
496 volcanic rocks on the West Greenland continental margin: volcanic evolution and event correlation to other parts
497 of the North Atlantic Igneous Province: *Geological Magazine*, vol. 153, pp. 487–511,
498 doi:10.1017/s0016756815000515.
- 499 Li, Z. X., Bogdanova, S. V., Collins, A. S., Davidson, A., Waele, B. D., Ernst, R. E., Fitzsimons, I. C. W., Fuck,
500 R. A., Gladkochub, D. P., Jacobs, J., Karlstrom, K. E., Lu, S., Natapov, L. M., Pease, V., Pisarevsky, S. A.,
501 Thrane, K., and Vernikovsky, V., 2008, Assembly, configuration, and break-up history of Rodinia: a synthesis:
502 *Precambrian Research*, vol. 160, pp. 179–210, doi:10.1016/j.precamres.2007.04.021.
- 503 Loewen, M. W., Duncan, R. A., Kent, A. J. R., and Krawl, K., 2013, Prolonged plume volcanism in the Caribbean
504 large igneous province: New insights from Curaçao and Haiti: *Geochemistry, Geophysics, Geosystems*, vol. 14,
505 pp. 4241–4259, doi:10.1002/ggge.20273.
- 506 Macdonald, F. A., Schmitz, M. D., Crowley, J. L., Roots, C. F., Jones, D. S., Maloof, A. C., Strauss, J. V., Cohen,
507 P. A., Johnston, D. T., and Schrag, D. P., 2010, Calibrating the Cryogenian: *Science*, vol. 327, pp. 1241–1243,
508 doi:10.1126/science.1183325.
- 509 Macdonald, F. A., Swanson-Hysell, N. L., Park, Y., Lisiecki, L., and Jagoutz, O., 2019, Arc-continent collisions in
510 the tropics set Earth's climate state: *Science*, vol. 364, pp. 181–184, doi:10.1126/science.aav5300.
- 511 Macdonald, F. A. and Wordsworth, R., 2017, Initiation of Snowball Earth with volcanic sulfur aerosol emissions:
512 *Geophysical Research Letters*, vol. 44, pp. 1938–1946, doi:10.1002/2016GL072335.
- 513 MacLennan, S. A., Park, Y., Swanson-Hysell, N. L., Maloof, A. C., Schoene, B., Gebreslassie, M., Antilla, E.,
514 Tesema, T., Alene, M., and Haileab, B., 2018, The arc of the Snowball: U-Pb dates constrain the Islay anomaly
515 and the initiation of the Sturtian glaciation: *Geology*, vol. 46, pp. 539–542, doi:10.1130/G40171.1.
- 516 Maher, K. and Chamberlain, C. P., 2014, Hydrologic regulation of chemical weathering and the geologic carbon
517 cycle: *Science*, vol. 343, pp. 1502–1504, doi:10.1126/science.1250770.
- 518 Manabe, S., 1969, Climate and the ocean circulation: the atmospheric circulation and the hydrology of the Earth's
519 surface: *Monthly Weather Review*, vol. 97, pp. 739–774, doi:10.1175/1520-0493(1969)097<739:catoc>2.3.co;2.
- 520 Michel, L. A., Tabor, N. J., and Montañez, I. P., 2016, Paleosol diagenesis and its deep-time paleoenvironmental
521 implications, Pennsylvanian-Permian Lodève Basin, France: *Journal of Sedimentary Research*, vol. 86, pp.
522 813–829, doi:10.2110/jsr.2016.41.
- 523 Montañez, I. P., 2013, Modern soil system constraints on reconstructing deep-time atmospheric co₂: *Geochimica et
524 Cosmochimica Acta*, vol. 101, pp. 57–75, doi:10.1016/j.gca.2012.10.012.
- 525 Murphy, J. B., van Staal, C. R., and Keppie, J. D., 1999, Middle to late Paleozoic Acadian orogeny in the northern
526 Appalachians: A Laramide-style plume-modified orogeny?: *Geology*, vol. 27, pp. 653–656,
527 doi:10.1130/0091-7613(1999)027<653:mtlpa>2.3.co;2.

- 528 Park, Y., Swanson-Hysell, N. L., MacLennan, S. A., Maloof, A. C., Gebreslassie, M., Tremblay, M. M., Schoene, B.,
529 Alene, M., Anttila, E., Tesema, T., and Haileab, B., in review, The lead-up to the Sturtian Snowball Earth:
530 Neoproterozoic chemostratigraphy time-calibrated by the Tambien Group of Ethiopia: GSA Bulletin.
- 531 Pirajno, F. and Hoatson, D. M., 2012, A review of Australia's large igneous provinces and associated mineral
532 systems: Implications for mantle dynamics through geological time: Ore Geology Reviews, vol. 48, pp. 2–54,
533 doi:10.1016/j.oregeorev.2012.04.007.
- 534 Pujol, M., Marty, B., Burgess, R., Turner, G., and Philippot, P., 2013, Argon isotopic composition of Archaean
535 atmosphere probes early Earth geodynamics: Nature, vol. 498, pp. 87–90, doi:10.1038/nature12152.
- 536 Ricci, J., Quidelleur, X., Pavlov, V., Orlov, S., Shatsillo, A., and Courtillot, V., 2013, New $^{40}\text{Ar}/^{39}\text{Ar}$ and K-Ar
537 ages of the Viluy traps (Eastern Siberia): Further evidence for a relationship with the Frasnian-Famennian mass
538 extinction: Palaeogeography, Palaeoclimatology, Palaeoecology, vol. 386, pp. 531–540,
539 doi:10.1016/j.palaeo.2013.06.020.
- 540 Schaller, M. F., Wright, J. D., and Kent, D. V., 2011, Atmospheric pCO₂ perturbations associated with the Central
541 Atlantic Magmatic Province: Science, vol. 331, pp. 1404–1409, doi:10.1126/science.1199011.
- 542 Schaller, M. F., Wright, J. D., Kent, D. V., and Olsen, P. E., 2012, Rapid emplacement of the Central Atlantic
543 Magmatic Province as a net sink for CO₂: Earth and Planetary Science Letters, vol. 323–324, pp. 27–39,
544 doi:10.1016/j.epsl.2011.12.028.
- 545 Schoene, B., Samperton, K. M., Eddy, M. P., Keller, G., Adatte, T., Bowring, S. A., Khadri, S. F. R., and Gertsch,
546 B., 2014, U-Pb geochronology of the Deccan Traps and relation to the end-Cretaceous mass extinction: Science,
547 vol. 347, pp. 182–184, doi:10.1126/science.aaa0118.
- 548 Shevenell, A. E., 2004, Middle Miocene Southern Ocean cooling and Antarctic cryosphere expansion: Science, vol.
549 305, pp. 1766–1770, doi:10.1126/science.1100061.
- 550 Swanson-Hysell, N. L., Kilian, T. M., and Hanson, R. E., 2015, A new grand mean palaeomagnetic pole for the 1.11
551 Ga Umkondo large igneous province with implications for palaeogeography and the geomagnetic field:
552 Geophysical Journal International, vol. 203, pp. 2237–2247, doi:10.1093/gji/ggv402.
- 553 Swanson-Hysell, N. L. and Macdonald, F. A., 2017, Tropical weathering of the Taconic orogeny as a driver for
554 Ordovician cooling: Geology, vol. 45, pp. 719–722, doi:10.1130/G38985.1.
- 555 Swanson-Hysell, N. L., Ramezani, J., Fairchild, L. M., and Rose, I. R., 2019, Failed rifting and fast drifting:
556 Midcontinent Rift development, Laurentia's rapid motion and the driver of Grenvillian orogenesis: GSA Bulletin,
557 doi:10.1130/b31944.1.
- 558 Thorne, J., Cooper, M., and Claoué-Long, J., 2014, Guide to using the Australian mafic-ultramafic magmatic
559 events GIS dataset: Archean, Proterozoic and Phanerozoic magmatic events: Geoscience Australia,
560 doi:10.11636/record.2014.039.
- 561 Torsvik, T. H. and Cocks, L. R. M., 2016, Earth History and Palaeogeography: Cambridge University Press,
562 doi:10.1017/9781316225523.
- 563 Trenberth, K. E., Fasullo, J. T., and Mackaro, J., 2011, Atmospheric moisture transports from ocean to land and
564 global energy flows in reanalyses: Journal of Climate, vol. 24, pp. 4907–4924, doi:10.1175/2011jcli4171.1.
- 565 Trenberth, K. E., Stepaniak, D. P., and Caron, J. M., 2000, The global monsoon as seen through the divergent
566 atmospheric circulation: Journal of Climate, vol. 13, pp. 3969–3993,
567 doi:10.1175/1520-0442(2000)013<3969:tgmast>2.0.co;2.
- 568 West, A. J., 2012, Thickness of the chemical weathering zone and implications for erosional and climatic drivers of
569 weathering and for carbon-cycle feedbacks: Geology, vol. 40, pp. 811–814, doi:10.1130/g33041.1.

- 570 Xu, Y.-G., Wei, X., Luo, Z.-Y., Liu, H.-Q., and Cao, J., 2014, The Early Permian Tarim large igneous province:
571 Main characteristics and a plume incubation model: *Lithos*, vol. 204, pp. 20–35, doi:10.1016/j.lithos.2014.02.015.
- 572 Zhai, Q.-g., Jahn, B.-m., Su, L., Ernst, R. E., Wang, K.-l., Zhang, R.-y., Wang, J., and Tang, S., 2013, SHRIMP
573 zircon U-Pb geochronology, geochemistry and Sr-Nd-Hf isotopic compositions of a mafic dyke swarm in the
574 Qiangtang terrane, northern Tibet and geodynamic implications: *Lithos*, vol. 174, pp. 28–43,
575 doi:10.1016/j.lithos.2012.10.018.
- 576 Zhou, M.-F., Malpas, J., Song, X.-Y., Robinson, P. T., Sun, M., Kennedy, A. K., Lesher, C., and Keays, R. R.,
577 2002, A temporal link between the Emeishan large igneous province (SW China) and the end-Guadalupian mass
578 extinction: *Earth and Planetary Science Letters*, vol. 196, pp. 113–122, doi:10.1016/s0012-821x(01)00608-2.
- 579 Zhu, D.-C., Chung, S.-L., Mo, X.-X., Zhao, Z.-D., Niu, Y., Song, B., and Yang, Y.-H., 2009, The 132 Ma
580 Comei-Bunbury large igneous province: Remnants identified in present-day southeastern Tibet and southwestern
581 Australia: *Geology*, vol. 37, pp. 583–586, doi:10.1130/g30001a.1.